Progress in Earth and Planetary Science

RESEARCH ARTICLE Open Access

# Development of a global sediment dynamics model

Misako Hatono[1,2*] and Kei Yoshimura[3]

## Abstract

Sediment dynamics play an important role in various aspects of earth system modeling. In this study, we developed a global sediment dynamics model that considers suspended sediment and bedload at short timescales. We validated suspended sediment from four observation stations in the Amazon River basin and over 60 observation stations from around the world based on a variable criteria such as availability of data samples. Our model was able to effectively reproduce seasonality and spatial distribution of suspended sediment flow. However, our global estimate of approximately 4 Bt/a was significantly lower than previous estimates; therefore, we discuss potential causes of this discrepancy, including target time period and discrepancies with previous extrapolated methods. Our newly developed sediment dynamics model could provide a better understanding of global sediment transfer and contributes to various related research fields such as coastal modeling and natural disasters.

**Keywords:** Global sediment dynamics, Suspended sediment flow, Amazon River basin, Oceania

## 1 Introduction

Rivers play a large role in material transport as well as in the water cycle. Sediments flowing through rivers carry various nutrients and are thus vital in the transport of various materials such as carbon and nitrogen from land to the oceans (Walling 2006). Movement of sediments in the rivers can be affected by a wide range of factors such as dam construction and major flood events. Construction of large dams such as the Madeira Hydroelectric Complex resulted in a 30% decrease of fine suspended sediment concentration (Rivera et al. 2019), while Three Gorges Reservoir led to a 98.7% decrease of multi-year mean annual sediment deposition in a downstream lake (Zhou et al. 2016). Walling (2006) stated rivers such as Rio Magdalena and Fly River saw significant increases in sediment flow due to human activities such as land clearance and mining. Kao and Milliman (2008) stated a river in Taiwan increased its sediment flow significantly when an intense typhoon hit the river basin, while Horowitz (2010) showed a sharp decrease in suspended sediment concentration after a large flood in the Mississippi River basin which may be because large amounts of bedload storage was removed due to the flood. These changes in sediment flow could be amplified as flood frequency and intensity have been predicted to increase with climate change (Hirabayashi et al. 2013).

Sediment-related studies using various methods such as modeling, observations and remote sensing including those mentioned above have long been conducted on a relatively local scale, focusing on a specific river basin or shoreline (Blum and Roberts 2009; Shrestha et al. 2013; Yu et al. 2013; Park and Latrubesse 2014). This is partly because sediment movement and its governing factors depend largely on regional characteristics such as river discharge, basin area, lithology, and anthropogenic activities (Milliman and Farnsworth 2011). To account for contributing factors in a given basin, many regional models are calibrated using observation data to accurately represent the spatial and temporal characteristics of sediment flow (e.g., Bourgoin et al. 2007; Rostamian et al. 2008; Cohen et al. 2013). The

* Correspondence: misakohatono@hiroshima-u.ac.jp
[1]School of Engineering, Tohoku University, 6-6-06 Aoba, Aramaki, Aoba, Sendai, Miyagi 980-8579, Japan
[2]Graduate School of Advanced Science and Engineering, Hiroshima University, 1-4-1 Kagamiyama, Higashi-Hiroshima City, Hiroshima 739-8527, Japan
Full list of author information is available at the end of the article

lack of sufficient observation data regarding sediments worldwide limits the potential target area of these regional models. It is said less than 10% of sediment flow to the oceans is measured (Cohen et al. 2013), whereas river discharge is measured in over 70% of rivers flowing to the oceans (Fekete and Vörösmarty 2007).

A robust understanding of sediment dynamics at larger scales which would allow for intra-basin comparisons (e.g., Cohen et al. 2014) may compensate for the lack of detailed regional studies in various parts of the world. Previous studies have collected observation data worldwide and analyzed the relationship between sediment-related variables and regional characteristics (e.g., Holeman 1968; Milliman and Farnsworth 2011). Panin (2004) compiled 30 global estimates of sediment flow to the oceans using previous studies from 1950 and afterwards. Although the estimates contain uncertainty, recent estimates in their database have been in the range of 13.5–22 Bt/a. Nearly all of the estimates in Panin (2004) and subsequent studies (e.g., Milliman and Farnsworth 2011; Syvitski 2011) are based on limited observations and a simple extrapolation based on few variables, such as basin area and geological parameters. Due to lack of data availability, several of these studies used estimates from a single river basin, the Mississippi River, to extrapolate to global estimates proportionate to land area (e.g., Gilluly 1955; Mackenzie and Garrels 1966). With the increase of available observation data worldwide, Holeman (1968) was one of the first studies included in Panin (2004) to compile annual suspended sediment flow from various studies in all continents. They conducted simple extrapolation to the global estimate by assuming it is proportionate to the drainage area of rivers in their database which ranged from 1500 to 6,000,000 $km^2$. With this approach, continuous efforts to compile up-to-date observation data from various research organizations worldwide must be conducted to achieve observation-based global estimates that reflect changes in sediment flow over time.

Since achieving sufficient observations at larger scales using homogenous measuring techniques can be extremely difficult (Mouyen et al. 2018), numerical simulations are often used. Previous studies attempted to estimate long-term suspended sediment flow or yield using several key parameters. Syvitski and Milliman (2007) developed the BQART model which estimates the fluvial sediment flux from a basin as a function of parameters such as geological and human factors, river discharge, basin area, maximum relief, and basin averaged temperature. Pelletier (2012) developed a model that estimates long-term sediment flow and yield at the global scale at 5 arc min spatial resolution. They considered sediment detachment in hillslopes and used the Rouse number to determine whether the sediment is routed to the downstream pixel. There have also been several studies aimed to incorporate sediment processes into Earth System Model frameworks at shorter time periods (e.g., Naipal et al. 2016; Tan et al. 2018), but none that explicitly estimates the movement of both suspended sediment and bedload. Cohen et al. (2013) developed WBMsed, which is one of the few distributed global-scale sediment models to estimate suspended sediment flow at a daily timescale. Although their simulations showed good accuracy in the long-term average of global river basins and daily fluctuation of rivers in the USA, the main limitation of WBMsed is that it uses the Psi model (Morehead et al. 2003) to estimate the daily fluctuation from long-term average sediment flow and does not explicitly model sediment dynamics at daily timescales.

In this study, we aim to overcome this limitation and calculate various aspects of sediment transport in rivers including bedload at short timescales. The following sections describe our newly developed global sediment dynamics model and validation results using a new global sediment-related observation database. We also conducted sensitivity analysis on multiple parameters within our model and investigated discrepancies in global sediment flow estimates between our model simulations and previously reported values such as those included in Panin (2004).

## 2 Methods/experimental

### 2.1 Model framework

Our global sediment dynamics model was developed within a framework called Integrated Land Simulator (ILS; Nitta et al. submitted), which consists mainly of a land surface model MATSIRO (Takata et al. 2003), a river inundation model CaMa-Flood (Yamazaki et al. 2011, 2013), and a coupler Jcup (Arakawa et al. 2011). As Jcup can exchange variables and communicate between different grid coordinates, this framework makes it easier to use various forcing and boundary data and to combine different models. In this study, only CaMa-Flood and Jcup are used.

Sediment dynamics are incorporated in a global physically based river routing model known as CaMa-Flood, which calculates river hydrodynamics including floodplain inundation—using river runoff from land surface models as the input. Each grid consists of a unit catchment represented by subgrid topography parameters. The model uses the local inertial equation proposed by Bates et al. (2010) to calculate river discharge. A cumulative distribution function of the high-resolution elevation pixels included in each unit catchment is used to distinguish the elevation of every 10% of the floodplain in order to implicitly calculate the inundated area. The floodplain elevation profile in each grid is achieved by

sorting high-resolution elevation data from SRTM30. The river channel dimensions such as river width and river bed area used in sediment dynamics processes in the following subsection are also derived from the boundary data of CaMa-Flood. Details on the channel dimensions and the floodplain elevation profile are mentioned in Yamazaki et al. (2011). It should be noted the term "floodplain" in this study refers to all areas in each grid cell excluding the river channel, regardless of whether there is flooding or not. Notably, the sediment dynamics in this study are only incorporated into the river channel.

### 2.2 Sediment dynamics

Suspended sediment is sediment transported mainly by river flow, and bedload is sediment transported by tumbling and rolling near the river bed. Figure 1a provides a schematic in each grid of the sediment dynamics model. Each grid contains storage for suspended sediment and bedload which gets inflow from upstream grids and outflows to a downstream grid. Exchange between the suspended sediment and bedload storages are conducted by suspension and deposition. Sediment erosion is estimated to be used as input from the land.

The parameters included in the following processes were calibrated by trial and error using the suspended sediment transport measured by observation stations in the Amazon River basin (mainly Obidos, unless stated otherwise), unless stated otherwise. We chose the Amazon River basin because our observation database included stations relatively near the river mouth, which would be important when discussing suspended sediment flow to the oceans. Also, there were multiple observation stations within the basin which would allow for comparison of different characteristics within a basin. The sensitivity analysis for some of the calibrated parameters is discussed in the results section.

Sediment erosion ers [$m^3/km^2/h$] is given by

$$\mathrm{ers} = \beta \theta^c r^d \tag{1}$$

where $\theta$ is the slope [deg], $r$ is precipitation [mm/h], and $\beta$, $c$, $d$ are the constant coefficients (Sunada and Hasegawa 1994). $\beta$, $c$, and $d$ were calibrated to 0.1, 1, and 2 respectively. The slope and sediment erosion are calculated for every 10% of the floodplain elevation profile, and the aggregated sediment erosion is used as input to the rivers in each grid. Figure 1b shows a schematic of the slopes estimated from the floodplain elevation profile in CaMa-Flood. The elevation for every tenth percentile of the floodplain in each grid is prepared as the boundary data for CaMa-Flood. The slope for every tenth percentile of the floodplain $\theta_i$ [deg] is estimated as

$$\theta_i = \tan^{-1}\left(\frac{E_i - E_{i-1}}{B_{10}}\right) \cdot \frac{180}{\pi} \tag{2}$$

where $E_i$ is the elevation [$m$] of the tenth percentile $i$ and $B_{10}$ is the width for every tenth percentile [$m$] of the floodplain. $E_0$ is set to 0 since the floodplain elevation profile is defined as the height above the river channel.

The adopted fundamental equations for the following processes follow those of Hamaguchi et al. (2012). The processes involved in outflowing suspended sediment from any given grid are suspended sediment flow and deposition. Suspended sediment flow $Q_s'$ and deposition $DEP'$ can be written as

$$Q_s' = CQ = \frac{S_s}{S} Q \tag{3}$$

$$DEP' = w_f A C = w_f A \frac{S_s}{S} \tag{4}$$

where $C$ is the suspended sediment concentration [$m^3/m^3$] $S_s$ is the suspended sediment storage [$m^3$], $S$ is the river water storage [$m^3$], $Q$ is the river discharge [$m^3/s$],

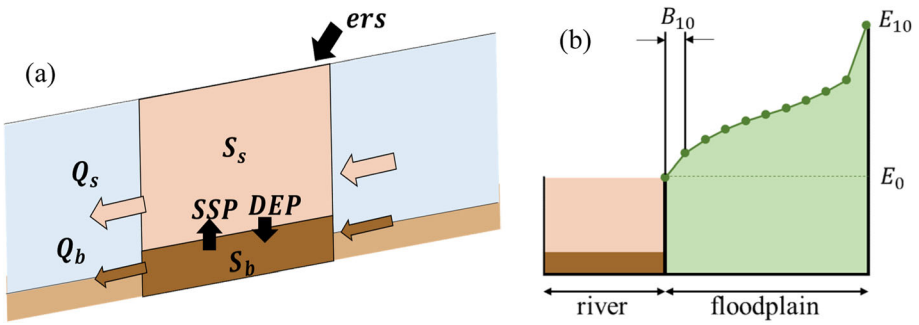


**Fig. 1** Schematic of **a** sediment dynamics in each grid and **b** estimated slopes of the floodplain. $S_s$, $S_b$, $Q_s$, and $Q_b$ are suspended sediment storage, bedload storage, suspended sediment flow, and bedload flow, respectively. SSP, DEP, and ers are suspension, deposition, and sediment erosion, respectively. $E_0$ and $E_{10}$ are the elevation [m] of river channel and last tenth percentile, respectively. $B_{10}$ is the width for every tenth percentile [m] of the floodplain

$w_f$ is the setting velocity calculated from Rubey (1933), and $A$ is the river bed area [m$^2$]. River bed area is calculated by multiplying river width and length used in CaMa-Flood. Following Liston et al. (1994), we assumed that sediment outflow is proportional to sediment storage to avoid unstable calculations when the storage is exceeded by outflow from a certain grid. The suspended sediment outflow from a grid is the sum of suspended sediment flow and deposition. From Eqs. (3) and (4), the outflowing suspended storage change $\Delta S_{os}$ can be written as

$$\frac{dS_{os}}{dt} = -\left(a_q + a_p\right)S_s \tag{5}$$

$$\Delta S_{os} = \left(1 - e^{-\left(a_q + a_p\right)\Delta t}\right)S_s \tag{6}$$

where $a_q = \frac{Q}{S}$ and $a_p = \frac{w_f \mathrm{A}}{S}$. By assuming that the storage change can be proportionally attributed to each of the factors, suspended sediment flow $Q_s$ [m$^3$/s] and deposition DEP [m$^3$/s] is estimated in our model as

$$Q_s = \frac{a_q}{a_q + a_q}\frac{\Delta S_{os}}{\Delta t} \tag{7}$$

$$\mathrm{DEP} = \frac{a_p}{a_q + a_p}\frac{\Delta S_{os}}{\Delta t} \tag{8}$$

It should be noted the unit of suspended sediment flow is converted to mass (e.g., tons/day) in the analysis by assuming the specific gravity of sediment is 2.65.

The outflowing bedload from a given grid includes bedload flow and suspension. Bedload flow $Q_b^{'}$ (Ashida and Michiue 1972) and suspension SSP$^{'}$ can be written as

$$Q_b^{'} = 17B\sqrt{sgD^3}\tau_{*e}^{\frac{3}{2}}\left(1 - \frac{\tau_{*c}}{\tau_*}\right)\left(1 - \frac{u_{*c}}{u_*}\right) \tag{9}$$

$$\mathrm{SSP}^{'} = q_{su}A \tag{10}$$

where $B$ is the river width [m], $s$ is the specific gravity, $D$ is the sediment particle diameter [m], $u_*$ is the shear velocity, $u_{*c}$ is the critical shear velocity, $\tau_* = \frac{{u_*}^2}{sgd}$ is the critical shear stress, and $q_{\mathrm{su}}$ is suspending velocity estimated from Itakura (1984). Unlike suspended sediment outflow, the amount of storage is not a limiting factor in Eqs. (9) and (10). Therefore, we implemented a layer of bedload that interacts with the suspended sediment, known as an exchange layer. The volume of the exchange layer $S_e$ [m$^3$] is given by

$$S_e = \min(h_b A, S_b) \tag{11}$$

where $h_b$ is the thickness of the exchange layer [m] and $S_b$ is the total volume of bedload storage [m$^3$]. We set the thickness of the exchange layer to 0.05 mm which is the center size of the grain size classification. We assume that the sediment in the exchange layer is the upper limit of outflowing bedload at each time step and applied the exchange layer to bedload storage ratio to the original estimated values from Eqs. (9) and (10). Therefore, the outflowing change in exchange layer storage can be written as

$$\frac{dS_e}{dt} = -\left(b_q + b_s\right)S_e \tag{12}$$

$$\Delta S_e = \left(1 - e^{-\left(b_q + b_s\right)\Delta t}\right)S_e \tag{13}$$

where $b_q = \frac{Q_b^{'}}{S_b}$ and $b_s = \frac{SSP^{'}}{S_b}$. The equations above can be broken down to derive bedload flow $Q_b$ [m$^3$/s] and suspension SSP [m$^3$/s] as

$$Q_b = \frac{b_q}{b_q + b_s}\frac{\Delta S_b}{\Delta t} \tag{14}$$

$$\mathrm{SSP} = \frac{b_s}{b_q + b_s}\frac{\Delta S_b}{\Delta t} \tag{15}$$

The above-mentioned processes are calculated for each sediment type within each grid. Temporal changes in storage of each sediment type is given by

$$S_{si}^{t+\Delta t} = S_{si}^t + \sum_k^{\text{upstream}} Q_{sik}^t \Delta t - Q_{si}^t \Delta t + \mathrm{SSP}_i^t \Delta t - DEP_i^t \Delta t + \mathrm{ers}_i^t A_f \frac{\Delta t}{3600} \tag{16}$$

$$S_{di}^{t+\Delta t} = S_{di}^t + \sum_k^{\text{upstream}} Q_{bik}^t \Delta t - Q_{bi}^t \Delta t + \mathrm{DEP}_i^t \Delta t - SSP_i^t \Delta t \tag{17}$$

where $t$ is time, $\Delta t$ is the time step, $k$ is the index indicating each upstream grid for the targeted grid, $i$ indicates the sediment type, and $A_f$ is floodplain area [km$^2$].

Nihei et al. (2005) stated that suspended sediment concentration becomes vertically uniform during rising water periods, whereas near-bed suspended sediment concentrations exceed surface concentration at peaks and during decreasing water periods. We implemented a scheme to change the suspension and deposition coinciding with flow velocity change. Changes in the flow regimes are defined as

$$\text{Rising} : v_t \geq \frac{v_{t-1} + v_{t-2}}{2} + \mathrm{V} \tag{18}$$

$$\text{Peak/receding} : v_t < \frac{v_{t-1} + v_{t-2}}{2} + \mathrm{V} \tag{19}$$

where $v_t$ is the flow velocity [m/s] at time $t$ and $V$ is a constant value, which is set to 0.0005 m/s. We assume

that suspension increases when water is rising, and define $b_s$ in Eqs. (12)–(15) as

$$b_s = \alpha \frac{\mathrm{ssp}}{s_d} \tag{20}$$

where $\alpha$ is a constant value set to 10. When water is peaking or receding, we assume the suspended sediment concentration to have a vertical profile and apply an exponential function. The near-bed suspended sediment concentration is given by

$$C_b = \frac{6Z}{1 - e^{-6Z}} C \tag{21}$$

$$Z = \frac{w_f}{\kappa u_*} \tag{22}$$

and is substituted into $C$ of Eq. (4).

### 2.3 Boundary data and experimental settings

The developed sediment dynamics model uses precipitation and river runoff as input. We used precipitation from a global meteorological forcing dataset (Kim et al. 2009), which disaggregated observation based precipitation using reanalysis data time series, and obtained runoff from an off-line simulation of MATSIRO using Kim et al. (2009) as forcing data. The original forcing data was gridded at 1° spatial resolution with daily temporal resolution. Although there are various precipitation datasets, we used Kim et al. (2009) in order to maintain consistency with the river runoff data.

The initial value of bedload storage is the limit of river bed degradation. Implementing a constant value for all grids does not reflect regional characteristics, therefore we used data of depth to bedrock, as described by Shangguan et al. (2017). This dataset is made by combining various data such as publicly available soil profiles, borehole logs, and lithological maps using machine learning methods. The originally downloaded 1 km resolution was interpolated to match that of our experimental settings, 0.5° and multiplied by the grid area to determine the initial value of bedload storage. Grids having invalid values, for reasons such as differences in land-sea boundaries, were assigned the mean value of all grids.

Variously sized sediments are both mixed in the river bed and suspended in the river. We used three representative sizes for sand, silt, and clay to depict the mixed-sized sediments (Table 1). The sediment dynamics explained in the previous section are calculated individually for each sediment size, and we used the total suspended sediment flow of all three sediment sizes to validate our model outputs. We used sand, silt, and clay fractions from Hengl et al. (2014) to obtain the gridded distribution of each sediment size. The data from Hengl et al. (2014) represent the percentage of each sediment type in the land surface. We aggregated the original 1 km spatial resolution to match that of our experimental settings. For grids with no valid data for these three sediment sizes (e.g., Sahara Desert), we assumed that all three sizes existed evenly. These distributions were set as the distribution of sediment erosion at each time step and the initial value of bedload storage. Although the grain size distribution can be different between the land surface and bedload, we used this distribution for the initial value of bedload storage since the size distribution of bedload storage is extremely difficult to obtain at the global scale.

**Table 1** Representative diameter of three sediment sizes

| | Representative diameter [mm] | Size range [mm] |
|---|---|---|
| Sand | 1 | 0.05 < D < 2 |
| Silt | 0.025 | 0.002 < D < 0.05 |
| Clay | 0.001 | D < 0.002 |

The river and sediment dynamics model was calculated at 0.5° spatial resolution with a unit catchment assigned to each grid. The temporal resolution was determined to fit the Courant-Friedrichs-Lewy condition, which was approximately 15 min. The results in the following sections show daily and monthly averaged values. The initial water and suspended sediment storage is set as 0. Calculation was conducted for the period 1979–2000. The first 2 years were used as spin-up, and we analyzed a total of 20 years from 1981 to 2000. The control experiments that used parameter values stated in the previous section are referred to as CTL.

### 2.4 Observation data

Although many observations have been conducted for sediment-related research, most of them are conducted at a regional- or basin- scale; these observation data have not been compiled in a global database. We were able to gather sediment-related observation data from multiple sources to compile a global database of over 4000 observation stations worldwide. From the validation criteria in the following subsection, we validated suspended sediment flow and concentration using data from the Global Environmental Monitoring System (GEMS; United Nations Environment Programme 2018), Hydrology and Geochemistry of the Amazon Basin (HYBAM; http://www.ore-hybam.org), National Water Data Archive (Environment Canada; https://wateroffice.ec.gc.ca/) and the United States Geological Survey Sediment Data Portal (https://cida.usgs.gov/sediment/). River discharge was validated using data from the Global Runoff Data Centre (GRDC). Discharge data for most stations in this study were available at daily timesteps.

### 2.5 Selection of validation sites

All available data was utilized for the global scale validation. The accuracy of hydrological regimes such as river discharge is very important as sediment dynamics are calculated using these variables. Therefore, we included the number of data samples of river discharge as a criteria to select stations for sediment validation sites. In order to have enough samples to estimate the accuracy and account for seasonality, we used stations that had at least 365 and 12 samples within 1981 to 2000 of valid river discharge and sediment data, respectively. The difference in number of samples is because our river discharge data was mostly in daily timescales and many of our sediment data was in monthly timescales. The selected stations also should have overlapping periods of available river discharge and sediment data. Since our model simulations are conducted on a relatively coarse 0.5°spatial resolution, we used stations that were located in areas with an upstream area of over 10,000 km$^2$. Sixty-one observation sites meeting each of the above-mentioned criteria were selected for validation. The correlation coefficient of simulated river discharge at all selected stations was significant at the 99% level. The minimum and maximum numbers of sediment samples at an observation station within 1981 to 2000 were 12 and 7305, respectively. We are actively collecting more observation data which would lead to an increase in validation sites for our developed model.

## 3 Results

### 3.1 Amazon River

Data from four stations in the Amazon River basin—Serrinha, Porto Velho, Manacapuru and Obidos—were validated using data from HYBAM. Observed suspended sediment concentration and river discharge were used to calculate the observed suspended sediment flow. Figure 2e shows the location of each of the four stations. Serrinha and Porto Velho are located along tributaries of the Amazon River, Negro River, and Madeira River, respectively. Table 2 shows the coordinates, upstream area, and annual mean river discharge at the four stations. The observed mean annual suspended sediment flow at each station was 4, 310, 250, and 360 Mt/a, respectively. These values are estimated by linearly interpolating obtained observation values, which are three samples per month at most, to get the annual temporal distribution. The modeled mean annual suspended sediment flow at each station was approximately 30, 90, 230, and 410 Mt/a, respectively. Figure 2a–d shows the time series of the observation and simulated daily suspended sediment flow [10$^3$ t/day] of four observation stations in the Amazon River basin. This indicates that the values for the furthest station upstream, Serrinha, are largely overestimated. This is because although Negro River, the tributary which Serrinha is located, is known to have significantly lower sediment transport because it drains cratonic areas and rainforests (Latrubesse et al. 2005), our simulation

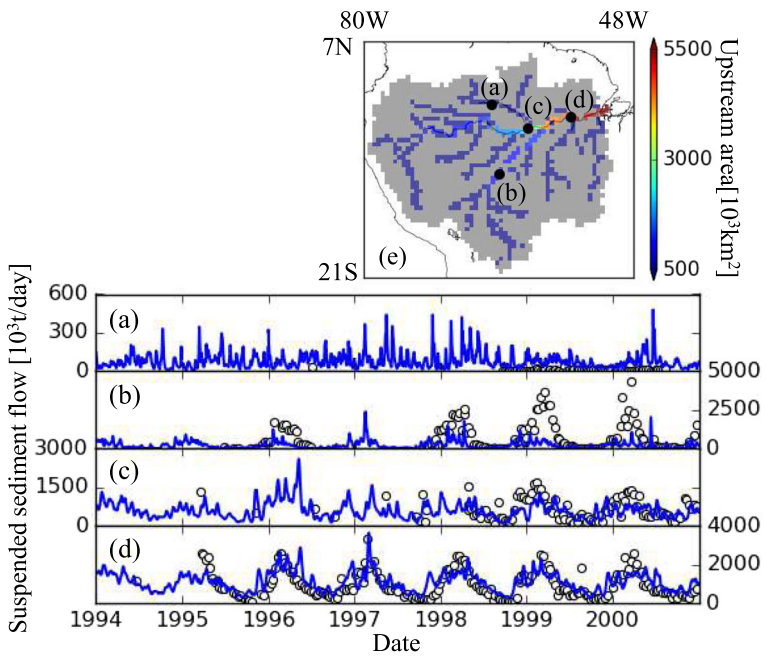


**Fig. 2** Daily suspended sediment flow [10$^3$ tons/day] at **a** Serrinha, **b** Porto Velho, **c** Manacapuru, and **d** Obidos. Black circle indicates observation, blue line indicates CTL simulation. **e** Basin map. The background color indicates upstream area [10$^3$ km$^2$]. Gray grids indicate grids whose upstream area is smaller than 50,000 km$^2$

**Table 2** Summary of validation stations in the Amazon River basin

| Station name | Coordinates (lon, lat) | Upstream area [$10^3$ $km^2$] | Mean annual river discharge [$m^3/s$] |
|---|---|---|---|
| Serrinha | (− 64.83, − 0.48) | 300 | 18,000 |
| Porto Velho | (− 63.92, − 8.74) | 1000 | 20,000 |
| Manacapuru | (− 60.61, − 3.31) | 2200 | 100,000 |
| Obidos | (− 55.51, − 1.95) | 4700 | 180,000 |

currently does not take into account geological features when estimating sediment erosion. Furthermore, the seasonal irregularities seen in the observation values require further investigation including observation uncertainty. Porto Velho showed large underestimation, but the seasonality was well represented. At Manacapuru and Obidos, both the fluctuation range and seasonality are well represented. The correlation coefficient for suspended sediment flow at Serrinha, Porto Velho, Manacapuru, and Obidos were 0.10, 0.49, 0.41, and 0.66, respectively. Partly due to our assumption that suspension increases in rising waters, our simulations have sharp daily fluctuations which are similar to the simulation results shown in Cohen et al. (2013).

Figure 3 shows the monthly breakdown of annual suspended sediment flow at each station. The width of each month is proportional to the monthly to annual ratio of suspended sediment flow. HYBAM had only up to three samples per month, so they were averaged for the monthly representative values. Due to the irregular monthly fluctuation in Serrinha, a clear peak is not present in the observation values. The remaining three stations showed one peak from winter to early spring, which are effectively simulated. Manacapuru and Obidos show a relatively similar monthly distribution. Although the model captures the characteristics of the distribution where sediment flow in January to April is larger compared to those in July to October, our model simulation does not have a distinct difference compared to the observation. Porto Velho, where more than half of the annual flow was concentrated in January to April, was distributed differently from the other stations in both the observation and model simulation. This characteristic is more obvious in the observation, where these 4 months account for almost 80% of the annual flow. The Madeira River, in which Porto Velho is located, experiences its flooding season from February to April and has widely fluctuating river discharge. Large amounts of sediment enter the river from the Andes during the flooding season, causing large concentrations in the earlier months of the year. Because of low river discharge in the upper basin grids in the model simulation, the high volume of sediment produced in mountainous areas cannot be delivered downstream, leading to a smaller proportion of sediment flow during the flooding season.

Our model simulation was able to capture the seasonality and peak timings of observation stations in the Amazon River basin which is one of the largest sources of suspended sediment flow to the oceans. This shows our global scale model has the capability to be used for individual basins.

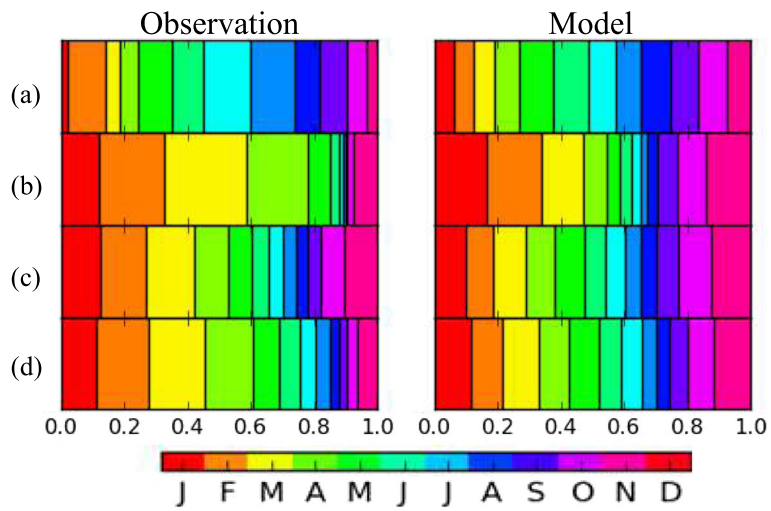


**Fig. 3** Monthly breakdown of annual suspended sediment flow. **a** Serrinha, **b** Porto Velho, **c** Manacapuru, **d** Obidos. Left column indicates observation, right column indicates CTL simulation

### 3.2 Global scale

Figure 4 shows the correlation coefficients of suspended sediment flow at 61 validation stations. Circles and triangles indicate stations where correlation coefficients are significant and insignificant, respectively, at the 95% significance level. Of the 61 validation stations worldwide, 55 stations had correlation coefficients that were significant at the 95% significance level and 20 stations had a positive Nash-Sutcliffe efficiency (NSE; Nash and Sutcliffe 1970). The high number of significant correlation coefficients indicates that the seasonality of suspended sediment flow is simulated well at our selected stations, but the peak values and/or fluctuation ranges may still need improvement since NSE, which is sensitive to observed and modeled means and variances (Legates and McCabe 1999), are relatively lower. The $R^2$ of NSE estimated for river discharge and suspended sediment flow individually at 61 stations was 0.23 ($p < 0.01$), which suggests accuracy of seasonality of river discharge does have a somewhat weak correlation with the accuracy of suspended sediment flow.

Figure 5 shows the month with the maximum suspended sediment flow. Forty-four out of the 61 validation stations that have at least 1 year with observation data in all 12 months were selected. Twenty-two stations had the same maximum month and the others were mostly within a 2-month bias. The exceptions were Serrinha in the Amazon River basin, a station along the Red River, 05OC001, a station along the Little Colorado River, 09402000, and a station along the Ohio River, 03294500. The observed maximums for Serrinha, 05OC001, 09402000, and 03294500 were February, April, February, and August, respectively, whereas the simulated maximums were May, July, June and January, respectively. Stations at high latitudes, like those in Russia and Canada, tend to have a peak at around May and June (Fig. 6a, b). Stations located in Mexico and the Mekong River basin, which have similar latitudes, peaked in July to September, later than the other selected stations (Fig. 6c, d). These characteristics are also apparent during the peak month of river discharge. Most of the stations showed a 0–2-month lag between river discharge and suspended sediment flow, which were present in the model simulations as well. Serrinha and Porto Velho in the Amazon River had longer lags of 3–4 months, which were not apparent in our model simulations.

The temporal trend of annual suspended sediment flow in CTL for global rivers with basin areas larger than 10,000 km$^2$ were assessed. The number of rivers that increased, decreased, or was stable over the 20 years was 58, 72, and 1022 rivers, respectively. The increasing and decreasing trends were significant at the 95% level. The distribution of trends were similar to the results in Walling and Fang (2003) which used 145 rivers in North America, Europe, and Asia. The temporal trend of the total suspended sediment flow to the oceans globally showed a decreasing trend.

Figure 7 shows the annual suspended sediment flow at river mouths for (a) rivers listed in Milliman and Farnsworth (2011) (hereafter referred to as MF11) and (b) 20 years average of CTL simulation. River mouths included in MF11 are shown in Fig. 7b. Rivers having a modeled annual discharge below 1 m$^3$/s are excluded in consideration of other rivers, mainly in the Oceania Region, that were simulated poorly due to the coarse resolution of the simulation and forcing data. Similar magnitudes of suspended sediment flow were simulated for regions like the Amazon and norther Eurasia, but those for southern and eastern Asia and western North America were underestimated, overall. MF11 has values from various studies so the uncertainty of the values in the literature must also be assessed in the future. For example, the Yellow River is among the largest suspended sediment supplies with 470 Mt/a; however, this value was calculated from only 5 sampling surveys from 1984 to 1986 (Zhang et al. 1994). It should also be noted that the data included in MF11

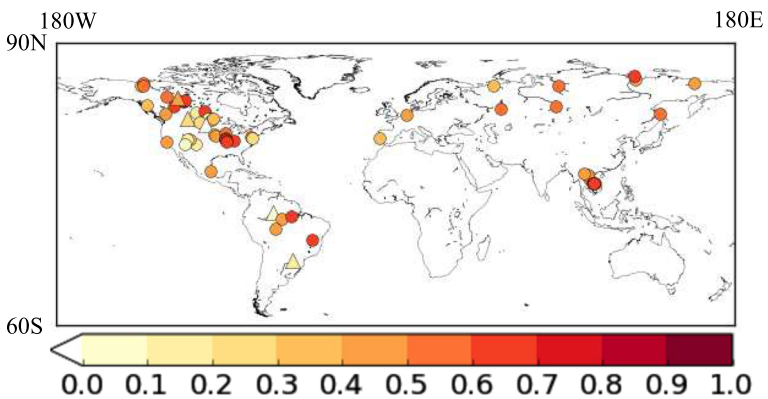


**Fig. 4** Correlation coefficient of suspended sediment flow. Circles and triangles indicate significance and insignificance at the 95% level, respectively

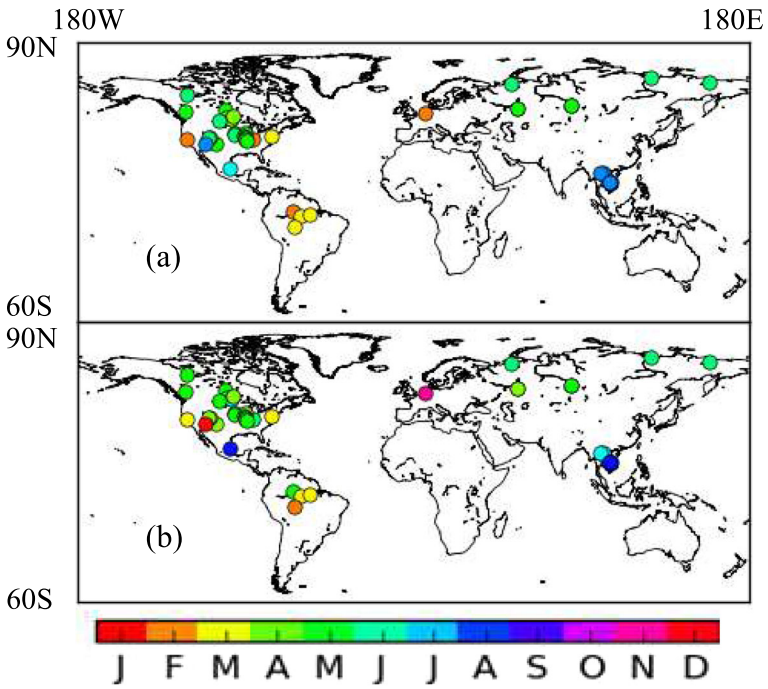


**Fig. 5** Month with the maximum suspended sediment flow. **a** Observation and **b** CTL simulation

are collected using various sampling techniques and sampling periods, so this may be a source of discrepancies between our results and MF11. The following section will discuss the legitimacy of using previous global estimates as the standard for validation. Figure 8 shows a direct comparison of MF11 and CTL simulation. The colors of each plot indicate the river basin area. The correlation and NSE were 0.88 and 0.57, respectively, indicating that the model simulations effectively captured spatial characteristics of global distribution. The total suspended sediment flow to the oceans from the plotted rivers of MF11 and model results were approximately 6.7 Bt/a and 2.8 Bt/a, respectively.

The amount of global suspended sediment transport from land to oceans has been reported in numerous studies, and recent estimates are approximately 13.5~22 Bt/a (Panin 2004). Panin (2004) states some studies have included suspended sediment flow due to anthropogenic effects in their estimates. The natural volume of sediment transport is approximately 6~12.6 Bt/a, and the anthropogenic sediment transport after the Anthropocene is estimated to be approximately 6.7~12 Bt/a. Our model estimates of approximately 4.0 Bt/a and appear to be of the same magnitude as the "natural" transport amount although it is still largely underestimated. Since our sediment dynamics model does not include

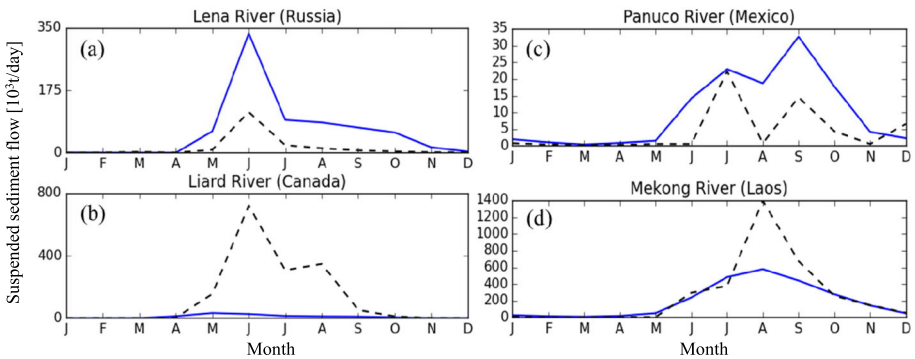


**Fig. 6** Averaged monthly suspended sediment flow [$10^3$ tons/day]. **a** Lena River, **b** Liard River, **c** Panuco River, and **d** Mekong River. Solid blue and dashed black lines indicate CTL simulation and observation data, respectively

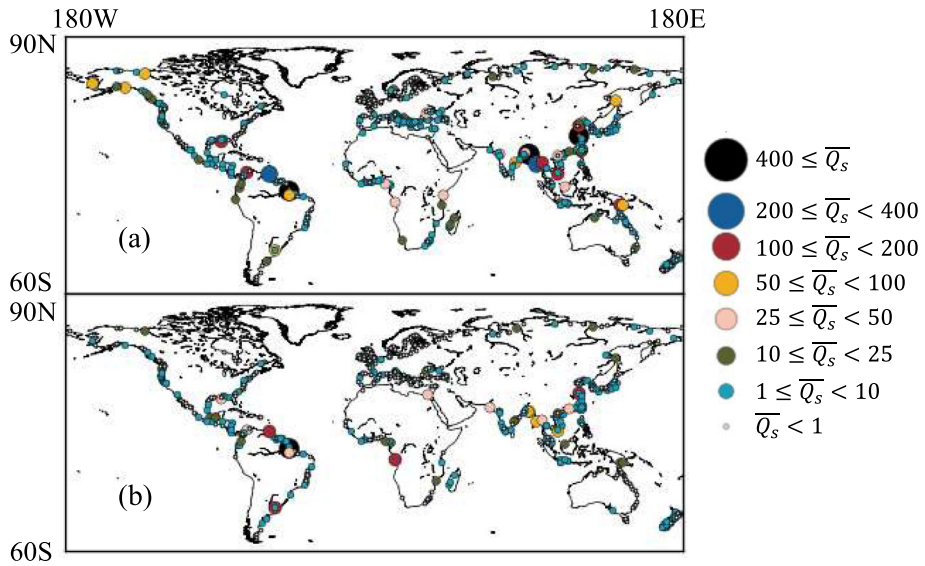


**Fig. 7** Annual suspended sediment flow [Mt/a]. **a** Milliman and Farnsworth (2011) and **b** CTL simulation

anthropogenic effects such as reservoirs and land use changes, we consider our estimates to be comparable to the "natural" transport amount.

Our model simulations were able to simulate the seasonality well at observation stations worldwide. Although our global suspended sediment flow to the oceans were significantly smaller compared to previous studies, we were able to capture the spatial distribution of sediments well. The following subsection introduces sensitivity analysis to some of our empirical parameters in order to assess the key factors to changes in suspended sediment flow.

### 3.3 Sensitivity analysis

Here, we checked the sensitivity to the empirical parameters considered in several processes in our model. The considered parameters and their CTL simulation and sensitivity experiment values are shown in Table 3. Figure 9 shows the suspended sediment flow at the Obidos station in the Amazon River basin. The solid and dashed blue lines indicate smaller and larger parameter values, respectively. The black solid line indicates CTL results and the black circles indicate HYBAM observation data. Increasing the erosion, exchange layer, and suspension parameters and decreasing the rising water parameter

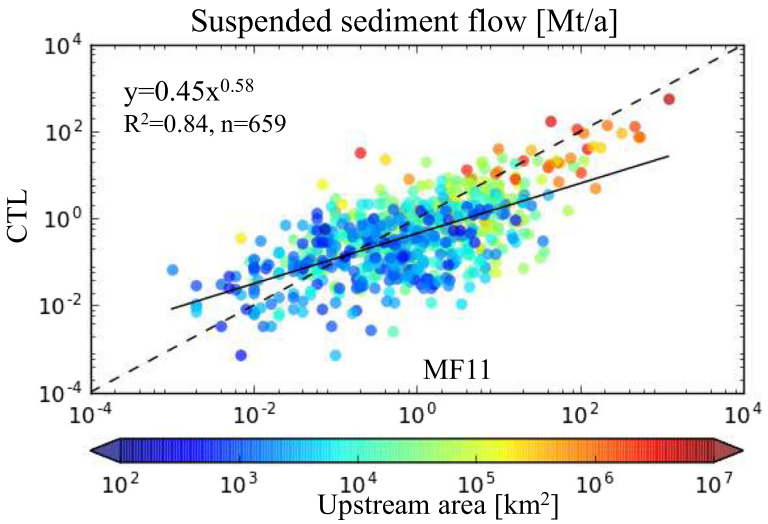


**Fig. 8** Scatter plot of annual suspended sediment flow [Mt/a] between MF11 and CTL. The colors of each plot indicate the river basin area. The solid and dashed line indicate the trend and 1:1 line, respectively

**Table 3** Parameter values for CTL and sensitivity simulations

| Related process | Variable/equation | CTL | Sensitivity simulation |
|---|---|---|---|
| Erosion | $\beta$ in Eq. (1) | 0.1 | 1, 0.01 |
| Exchange layer | $h_b$ in Eq. (11) | 0.00005 | 0.0005, 0.000005 |
| Rising waters | V in Eqs. (18), (19) | 0.0005 | 0.005, 0.00005 |
| Suspension | $a$ in Eq. (20) | 10 | 100, 1 |

lead to increased suspended sediment flow. The suspended sediment flow increases drastically when the erosion and exchange layer parameters are increased because these parameters directly increase the suspended sediment storage in each grid. Increasing the suspension parameter and decreasing the rising water parameter only slightly increases the suspended sediment flow because they affect only the suspended sediment in rising waters. Changing the parameters in the opposite way decreases the flow only slightly except for the sediment yield parameter, which reduced the suspended sediment flow to approximately half of CTL. These results indicate that sediment entering rivers because of land erosion affects the amount of suspended sediment flow in the Amazon River basin more than sediment being suspended from the bedload. The other three stations in the Amazon River basin used for validation had similar trends as well. These characteristics are different depending on basin characteristics and will be assessed globally in future studies.

The 20-year average of global suspended sediment flow from the river mouths from each sensitivity experiment ranged from 1.6 to 24 Bt/a. The lowest and highest estimates were when the sediment erosion parameter was decreased and increased, respectively. The trend of change due to increasing and decreasing the remaining three parameters were also similar to the changes described above for the Amazon River basin. When comparing the sensitivity at the continental scale, all of the continents except Africa were most sensitive to the erosion parameter by far, with the suspended sediment flow to the oceans ranging from approximately 0.1 to 8.3 times that in CTL. In Africa, the sensitivity to the erosion parameter was relatively smaller compared to other continents. From Eq. (1), the sensitivity to β of the erosion parameter can also be interpreted as sensitivity to the slope, which is a variable with some uncertainty since accurate representation of terrain slope at the global scale is difficult to obtain. Although these settings are not feasible for the Obidos station, we can ascertain the fluctuation range of global suspended sediment flow estimates from previous studies by adjusting the parameters with large uncertainty and relying on basin characteristics. This suggests a uniform value globally is not enough and parameters that sufficiently reflect various basin characteristics are necessary. Revising our parameters to enable consideration of regional characteristics without heavy calibration using observation data will be part of our future works.

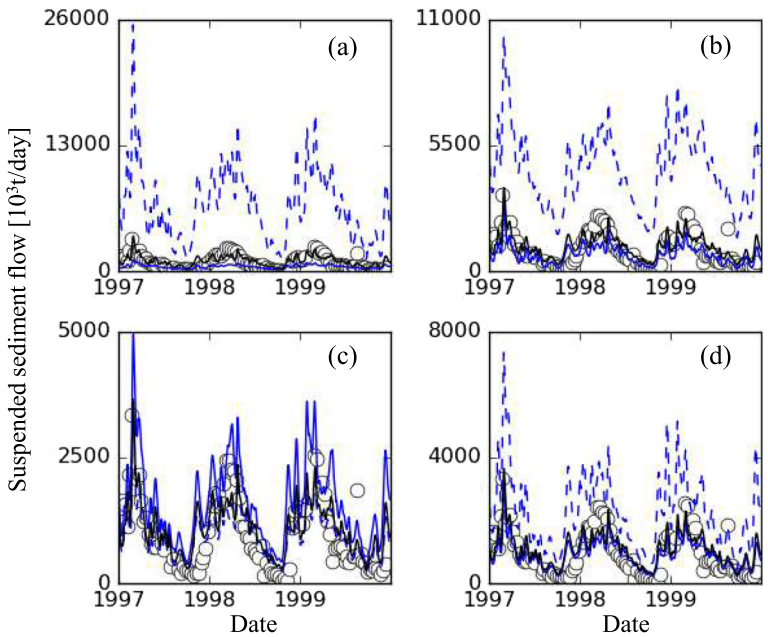


**Fig. 9** Daily suspended sediment flow [$10^3$ t/a] at Obidos station, as estimated from sensitivity experiments for **a** erosion, **b** exchange layer, **c** rising waters, and **d** suspension. Black circles and solid lines indicate observation and CTL simulations, respectively. Solid and dashed blue lines indicate smaller and larger parameter values, respectively

**Table 4** Statistics of simulations excluding sediment dynamics processes at Obidos

| | Sediment erosion | Suspension | Deposition | Bedload flow |
|---|---|---|---|---|
| Correlation coefficient | 0.69 | 0.99 | 0.99 | 1.00 |
| Average annual suspended sediment flow change[Mt/a] | − 350 | − 150 | + 1400 | $+ 1 \times 10^{-4}$ |

## 4 Discussion

All of the considered sediment dynamics processes in our model have an impact on the suspended sediment flow. We assessed the significance of each process to the suspended sediment flow by conducting simulations that exclude each of the following processes: sediment erosion, suspension, deposition, and bedload flow. The experimental settings are the same with CTL. Table 4 shows the change in average annual suspended sediment flow and correlation coefficient of each simulation at Obidos in the Amazon River basin. In order to assess the change compared to CTL, these statistics are estimated using suspended sediment flow of CTL as "observation." The change in average annual suspended sediment flow and correlation coefficient indicate change of the magnitude and seasonality of suspended sediment flow by excluding a certain process, respectively. Excluding bedload flow did not have a significant impact on the magnitude or seasonality of suspended sediment flow which is reasonable since it does not directly affect the suspended sediment storage. Also, bedload flow at Obidos station was several orders of magnitude smaller than suspended sediment flow and the other components in our simulation, which may be one of the reasons for the negligible impact. This indicates suspended sediment is the dominant source of sediment transport in rivers in our simulations. This finding is in agreement with previous studies (e.g., Milliman and Meade 1983). We found that the only simulation that had noticeable impact on the seasonality was when we excluded sediment erosion. This may be because while the other variables along with suspended sediment flow are more or less influenced by hydraulic variables in the river, estimation of sediment erosion does not share any variables with that of suspended sediment flow. Improving our sediment erosion process could lead to an improvement in the seasonality of suspended sediment flow in our simulations. The change of average annual suspended sediment flow was largest when deposition was excluded. This indicates that deposition is the key factor to the amount of suspended sediment flow in our simulations at Obidos. The global suspended sediment to the oceans when excluding sediment erosion, suspension, deposition, and bedload flow were 1.4, 2.7, 15.7, and 4.0 Bt/a, respectively. The relative magnitude of the change in the global scale was similar to that of Obidos. These findings from this analysis offer insight to the significance of each considered process and how to improve our model simulations.

Cohen et al. (2013) conducted validation on their simulation using WBMsed at the global scale using long-term average data from Syvitski and Milliman (2007) and at the regional scale for 11 USGS stations. They used 95 rivers for the global scale validation that were selected based on basin area and its consistency with the model's river network. By using the same criteria, we selected 403 rivers in MF11. The $R^2$ of global long-term average suspended sediment flow in WBMsed and our simulation was 0.66 and 0.82, respectively. Their simulations reported an overall underestimation for the 95 rivers, whereas our simulation did not have a clear trend. Both models showed underestimation in similar regions (e.g., East Asia, Mediterranean basin and northwestern North America). As for the regional scale, a USGS station along Illinois River, 05586100, was included in both our study and Cohen et al. (2013). Table 5 shows $R^2$ of daily river discharge and suspended sediment flow at this station for WBMsed and our CTL simulation. It should be noted their validation period was from 1997 to 2007, and also that their simulations for the USA was conducted at a 0.1° spatial resolution. Our sediment seasonality had better accuracy compared to WBMsed which may be due to better accuracy in river discharge since their daily fluctuation of sediment flow relies heavily on daily fluctuation of river discharge. It seems our simulation underestimates suspended sediment flows during peak discharge periods compared to WBMsed, but a more detailed comparison may be necessary as WBMsed seems to overestimates peak river discharge compared to our model. Model intercomparison using same forcing data will be part of future works.

As shown in the previous section, suspended sediment from land to the oceans is largely underestimated in comparison with the global database MF11. The previous global estimates are based on a compilation of numerous observational data that was extrapolated to fit the total area of a specific target area. Table 6 compares our CTL results of suspended sediment transport to oceans for different continents with those of MF11, (Syvitski et al. (2005) and Holeman (1968)). The suspended sediment flow in all of the continents except

**Table 5** $R^2$ of daily discharge and sediment flow for WBMsed and CTL

| | Discharge | Sediment |
|---|---|---|
| WBMsed (Cohen et al. 2013) | 0.48 | 0.35 |
| CTL | 0.56 | 0.53 |

**Table 6** Comparison between previous estimates and CTL of continental-scale suspended sediment flow [Bt/a]

| | MF11 | Syvitski et al. (2005) | Holeman (1968) | CTL |
|---|---|---|---|---|
| North America | 1.9 | 1.9 | 1.8 | 0.3 |
| South America | 2.3 | 2.5 | 1.1 | 1.1 |
| Africa | 1.5 | 0.8 | 0.5 | 0.4 |
| Europe | 0.85 | 0.7 | 0.4 | 0.1 |
| Asia | 12.55 | 6.8 | 14.5 | 1.9 |
| Total | 19.1 | 12.6 | 18.2 | 3.9 |
| Total (excluding Asia) | 6.55 | 5.8 | 3.7 | 2.0 |

Asia are larger in MF11 compared to Holeman (1968), which is partly due to the increase in number of data samples. It should be noted that Holeman (1968)'s estimates for Asia do not include Oceania due to lack of observation data. Our CTL results in South America, Africa, and Europe are relatively similar to the estimates by Holeman (1968). The underestimation in North America comes from the underestimation of Mississippi River basin and northwestern region of North America. The main source of the large underestimation in our global suspended sediment flow estimates is Asia, specifically Oceania. MF11 states that half of the suspended sediment from Asia comes from the Oceania islands, which account for 6800 Mt/a in just a few percent of the Earth's total land surface area. While our model results show obvious underestimations for some continents, there are also discrepancies in the previous studies. By comparing our model results with global long-term estimates and regional time series data, we consider the following as the two main causes of underestimation.

First, the previous global estimates are based on various observational studies that do not necessarily match the target period in this study. For example, the suspended sediment flow of the Amazon River in MF11, 1200 Mt/a, is based on estimates by Meade et al. (1985). Previous studies published in different decades (e.g., Holeman 1968; Meade et al. 1979) gave different estimates ranging between approximately 400 Mt/a and 1000 Mt/a. To estimate the recent amount of suspended sediment flow, we obtained daily data by applying linear interpolation temporally to the HYBAM observation data from 1996 to 2000, consisting of approximately 3 samples per month. The results showed that the mean annual suspended sediment flow for the Obidos station in the Amazon was approximately 360 Mt/a, which are closer to estimates by Holeman (1968). Our CTL estimate was approximately 420 Mt/a. The reason for this decrease in the observed values is outside the scope of this study because numerous factors may cause the amount of suspended sediment flow to change. However, our analysis indicates that the sources of previous global estimates do not necessarily represent the target period of this study.

The second factor focuses on discrepancies within the extrapolated results. Due to the lack of sufficient observation data on suspended sediment flow at the global scale, almost all of the previous global estimates relied on extrapolating existing observation data by considering factors such as basin area and geological features. As shown in Table 6, most of the underestimation is from Asia. The total suspended sediment flow from the East Indies islands in CTL was 600 Mt/a. Thirteen rivers with data stored in MF11 were chosen for direct comparison. The only threshold was modeled annual mean river

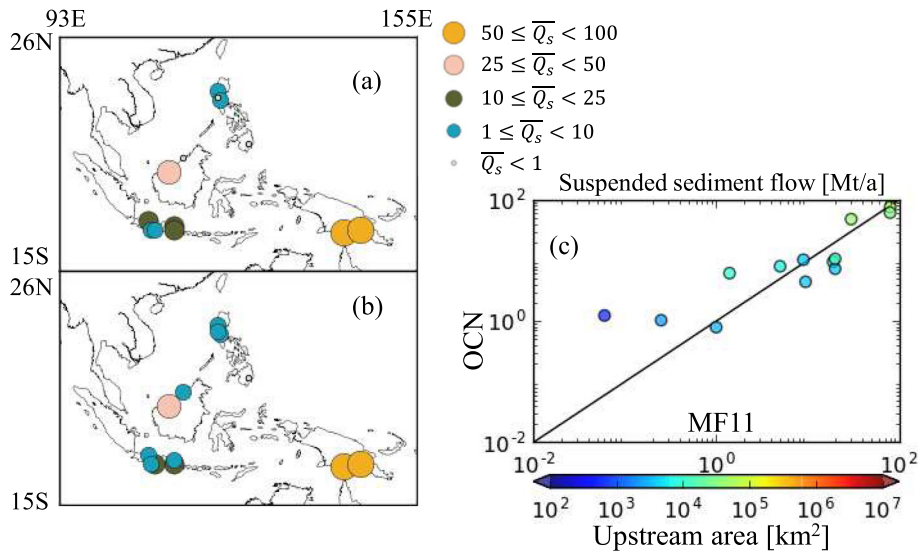


**Fig. 10** Comparison of suspended sediment flow [Mt/a] between MF11 and OCN simulation **a** MF11 **b** OCN, and **c** scatter plot

discharge is larger than 1 $m^3/s$. To discuss the regional characteristics and directly compare them with previous estimates, we calibrated the parameters to improve the accuracy for the selected river basins (hereafter referred to as OCN). The calibrated parameters are those included in calculating sediment erosion as Oceania is said to have a significantly high sediment yield (Milliman and Farnsworth 2011). Hereafter, we focus on comparing MF11 and OCN. Fig. 10 shows the distribution of suspended sediment flow in MF11 and OCN. The total suspended sediment flow of the 13 rivers for MF11, OCN, and CTL are approximately 290 Mt/a, 250 Mt/a, and 80 Mt/a, respectively. The root mean square error of OCN and CTL are 9 Mt/a and 25 Mt/a, respectively. The NSE of OCN and CTL is 0.88 and 0.09, respectively, which indicates the calibrated simulations of the suspended sediment flow of these rivers are significantly improved. Although the 13 recorded rivers are simulated well, the total suspended sediment flow for the entire Oceania region in MF11 and OCN are significantly different at 6800 Mt/a and 1900 Mt/a, respectively. Although our experimental settings, such as spatial resolution, may be responsible for this large difference, we must be careful when directly comparing previous extrapolated large-scale estimates with simulated results.

## 5 Conclusions

In this study, we developed a global sediment dynamics model in the framework of ILS. We were able to effectively represent the seasonality and magnitude of suspended sediment flow in numerous larger rivers. While individual rivers were well-represented, the global sum of suspended sediment flow was largely underestimated compared to previous global estimates. Two factors may be responsible for this underestimation: the difference in target time periods and the discrepancies among extrapolated results. These factors will be further investigated along with other improvements, such as considering an objective method for optimal global parameters and implementing the sediment dynamics in floodplains. This study will enable simulation of sediment dynamics at the global and regional scales for different time periods and will contribute to the understanding of sediment dynamics and its relationship with other earth system processes.

### Abbreviations

GEMS: Global Environment Monitoring System; GRDC: Global Runoff Data Centre; HYBAM: Hydrology and Geochemistry of the Amazon Basin; ILS: Integrated Land Simulator; NSE: Nash-Sutcliffe efficiency

### Acknowledgements

We would like to thank the originators of the suspended sediment flow and concentration data acquired through United Nations Environment GEMS/Water Progamme, HYBAM, National Water Data Archive, and United States Geological Survey. We would also like to thank the Global Runoff Data Centre for providing river discharge data.

### Authors' contributions

MH and KY conceived the topic. MH conducted the simulations and analysis. Both authors discussed the results and commented on the manuscript. Both authors read and approved the final manuscript.

### Authors' information

MH is currently an assistant professor at Hiroshima University. Parts of this study were conducted when MH was a postdoctoral fellow at Tohoku University. KY is a professor at the Institute of Industrial Science in The University of Tokyo.

### Funding

The sources of funding are: JSPS KAKENHI Grant Numbers JP18J00585, JP15J10456 and JP16H06291, Integrated Research Program for Advancing Climate Models (TOUGOU) Grant Number JPMXD0717935457 from the Ministry of Education, Culture, Sports, Science and Technology (MEXT), Japan and the Arctic Challenge for Sustainability II (ArCS II) Project (Program Grant Number JPMXD1420318865) from MEXT, Japan.

### Availability of data and materials

The data generated from our models may be available upon request from the corresponding author. The observation data used in this study are available from each corresponding organization.

### Competing interests

The authors declare that they have no competing interest.

### Author details

[1]School of Engineering, Tohoku University, 6-6-06 Aoba, Aramaki, Aoba, Sendai, Miyagi 980-8579, Japan. [2]Graduate School of Advanced Science and Engineering, Hiroshima University, 1-4-1 Kagamiyama, Higashi-Hiroshima City, Hiroshima 739-8527, Japan. [3]Institute of Industrial Science, The University of Tokyo, 5-1-5 Kashiwanoha, Kashiwa, Chiba 277-8574, Japan.

Received: 14 November 2019 Accepted: 31 August 2020
Published online: 07 October 2020

### References

Arakawa T, Yoshimura H, Saito F, Ogochi K (2011) Data exchange algorithm and software design of KAKUSHIN coupler Jcup. Procedia Computer Science 4: 1516–1525. https://doi.org/10.1016/j.procs.2011.04.164

Ashida K, Michiue M (1972) Study on hydraulic resistnace and bed-load transport rate in alluvial streams. Proceedings of the Japan Society of Civil Engineers 206:59–69. https://doi.org/10.2208/jscej1969.1972.206_59 (in Japanese)

Bates PD, Horritt MS, Fewtrell TJ (2010) A simple inertial formulation of the shallow water equations for efficient two-dimensional flood inundation modelling. J Hydrol 387:33–45. https://doi.org/10.1016/j.jhydrol.2010.03.027

Blum MD, Roberts HH (2009) Drowning of the Mississippi Delta due to insufficient sediment supply and global sea-level rise. Nat Geosci 2:488–491. https://doi.org/10.1038/ngeo553

Bourgoin LM, Bonnet M-P, Martinez J-M, Kosuth P, Cochonneau G, Moreira-Turcq P, Guyot JL, Vauchel P, Filizola N, Seyler P (2007) Temporal dynamics of water and sediment exchanges between the Curuaí floodplain and the Amazon River, Brazil. J Hydrol 335:140–156. https://doi.org/10.1016/j.jhydrol.2006.11.023

Cohen S, Kettner AJ, Syvitski JPM (2014) Global suspended sediment and water discharge dynamics between 1960 and 2010: Continental trends and intra-basin sensitivity. Glob Planet Chang 115:44–58. https://doi.org/10.1016/J.GLOPLACHA.2014.01.011

Cohen S, Kettner AJ, Syvitski JPM, Fekete BM (2013) WBMsed, a distributed global-scale riverine sediment flux model: Model description and validation. Comput Geosci 53:80–93. https://doi.org/10.1016/J.CAGEO.2011.08.011

Fekete BM, Vörösmarty CJ (2007) The current status of global river discharge monitoring and potential new technologies complementing traditional discharge measurements. In: Schertzer D, Hubert P, Koide S, Takeuchi K (eds) Predictions in Ungauged Basins: PUB Kick-off. IAHS publ, pp 129–136

Gilluly J (1955) Geologic contrasts between continents and ocean basins. In: Poldervaart A (ed) Crust of the Earth: A Symposium. Geological Society of America, pp 7–18

Hamaguchi T, Tanaka T, Kotsuki S, Tanaka K, Touge Y, Abe M (2012) Fundamental study on macro-scaled sediment yield/transport modeling based on

distributed runoff model. Annuals of Disaster Prevention Research Institute 55B:501–509 (in Japanese)
Hengl T, de Jesus JM, MacMillan RA, Batjes NH, Heuvelink GBM, Ribeiro E, Samuel-Rosa A, Kempen B, Leenaars JGB, Walsh MG, Gonzalez MR (2014) SoilGrids1km — Global soil information based on automated mapping. PLoS One 9:e105992. https://doi.org/10.1371/journal.pone.0105992
Hirabayashi Y, Mahendran R, Koirala S, Konoshima L, Yamazaki D, Watanabe S, Kim H, Kanae S (2013) Global flood risk under climate change. Nat Clim Chang 3:816–821. https://doi.org/10.1038/nclimate1911
Holeman JN (1968) The sediment yield of major rivers of the world. Water Resour Res 4:737–747. https://doi.org/10.1029/WR004i004p00737
Horowitz AJ (2010) A quarter century of declining suspended sediment fluxes in the Mississippi River and the effect of the 1993 flood. Hydrol Process 24:13–34. https://doi.org/10.1002/hyp.7425
Itakura T (1984) Study on turbulent diffusion in rivers. Reports of the Civil Engineering Research Institute 83:1–90 (in Japanese)
Kao SJ, Milliman JD (2008) Water and sediment discharge from small mountainous rivers, Taiwan: The roles of lithology, episodic events, and human activities. The Journal of Geology 116:431–448. https://doi.org/10.1086/590921
Kim H, Yeh PJF, Oki T, Kanae S (2009) Role of rivers in the seasonal variations of terrestrial water storage over global basins. Geophys Res Lett 36:2–6. https://doi.org/10.1029/2009GL039006
Latrubesse EM, Stevaux JC, Sinha R (2005) Tropical rivers. Geomorphology 70:187–206. https://doi.org/10.1016/j.geomorph.2005.02.005
Legates DR, McCabe GJ (1999) Evaluating the use of "goodness-of-fit" measures in hydrologic and hydroclimatic model validation. Water Resour Res 35:233–241. https://doi.org/10.1029/1998WR900018
Liston GE, Sud YC, Wood EF (1994) Evaluating GCM land surface hydrology parameterizations by computing river discharges using a runoff routing model: Application to the Mississippi Basin. J Appl Meteorol 33:394–405. https://doi.org/10.1175/1520-0450(1994)033<0394:EGLSHP>2.0.CO;2
Mackenzie FT, Garrels RM (1966) Chemical mass balance between rivers and oceans. Am J Sci 264:507–525. https://doi.org/10.2475/ajs.264.7.507
Meade RH, Dunne T, Richey JE, Santos UDM, Salati E (1985) Storage and remobilization of suspended sediment in the lower amazon river of Brazil. Science 228:488–490. https://doi.org/10.1126/science.228.4698.488
Meade RH, Nordin CF Jr, Curtis WF, Costa Rodrigues FM, Do Vale CM, Edmond JM (1979) Sediment loads in the Amazon River. Nature 278:161–163. https://doi.org/10.1038/278161a0
Milliman JD, Farnsworth KL (2011) River discharge to the coastal ocean: A global synthesis. Cambridge University Press, Cambridge
Milliman JD, Meade RH (1983) World-wide delivery of sediment to the oceans. The Journal of Geology 91:1–21. https://doi.org/10.1086/628741
Morehead MD, Syvitski JP, Hutton EWH, Peckham SD (2003) Modeling the temporal variability in the flux of sediment from ungauged river basins. Glob Planet Chang 39:95–110. https://doi.org/10.1016/S0921-8181(03)00019-5
Mouyen M, Longuevergne L, Steer P, Crave A, Lemoine JM, Save H, Robin C (2018) Assessing modern river sediment discharge to the ocean using satellite gravimetry. Nat Commun 9:3384. https://doi.org/10.1038/s41467-018-05921-y
Naipal V, Reick C, Van Oost K, Hoffmann T, Pongratz J (2016) Modeling long-term, large-scale sediment storage using a simple sediment budget approach. Earth Surface Dynamics 4:407–423. https://doi.org/10.5194/esurf-4-407-2016
Nash JE, Sutcliffe JV (1970) River flow forecasting through conceptual models part I - A discussion of principles. J Hydrol 10:282–290. https://doi.org/10.1016/0022-1694(70)90255-6
Nihei Y, Iida Y, Sato K (2005) High-resolution ADCP measurements on vertical structures of current and suspended solid in an urban river. Proceedings of Hydraulic Engineering 49:631–636. https://doi.org/10.2208/prohe.49.631 (in Japanese)
Panin A (2004) Land-ocean sediment transfer in palaeotimes, and implications for present-day natural fluvial fluxes. In: Golosov V, Belyaev V, Walling DE (eds) Sediment Transfer throught the Fluvial System. IAHS, Moscow, pp 115–124
Park E, Latrubesse EM (2014) Modeling suspended sediment distribution patterns of the Amazon River using MODIS data. Remote Sens Environ 147:232–242. https://doi.org/10.1016/j.rse.2014.03.013
Pelletier JD (2012) A spatially distributed model for the long-term suspended sediment discharge and delivery ratio of drainage basins. J Geophys Res Earth Surf 117:F02028. https://doi.org/10.1029/2011JF002129
Rivera IA, Cardenas EA, Espinoza-Villar R, Espinoza JC, Molina-Carpio J, Ayala JM, Gutierrez-Cori O, Martinez J-M, Filizola N (2019) Decline of Fine Suspended Sediments in the Madeira River Basin (2003–2017). Water 11:514. https://doi.org/10.3390/w11030514
Rostamian R, Jaleh A, Afyuni M, Mousavi SF, Heidarpour M, Jalalian A, Abbaspour KC (2008) Application of a SWAT model for estimating runoff and sediment in two mountainous basins in central Iran. Hydrological Sciences 53:977–988. https://doi.org/10.1623/hysj.53.5.977
Rubey W (1933) Settling velocities of gravel, sand, and silt particles. Am J Sci 25:325–338. https://doi.org/10.2475/ajs.s5-25.148.325
Shangguan W, Hengl T, Mendes de Jesus J, Yuan H, Dai Y (2017) Mapping the global depth to bedrock for land surface modeling. Journal of Advances in Modeling Earth Systems 9:65–88. https://doi.org/10.1002/2016MS000686
Shrestha B, Babel MS, Maskey S, van Griensven A, Uhlenbrook S, Green A, Akkharath I (2013) Impact of climate change on sediment yield in the Mekong River basin: A case study of the Nam Ou basin, Lao PDR. Hydrol Earth Syst Sci 17:1–20
Sunada K, Hasegawa N (1994) Study on a synthetic model for sediment routing in a mountainous river system. Proceedings of JSCE 485:37–44. https://doi.org/10.2208/jscej.1994.485_37 (in Japanese)
Syvitski JPM (2011) Global sediment fluxes to the Earth's coastal ocean. Appl Geochem 26:S373–S374. https://doi.org/10.1016/J.APGEOCHEM.2011.03.064
Syvitski JPM, Milliman JD (2007) Geology, geography, and humans battle for dominance over the delivery of fluvial sediment to the coastal ocean. The Journal of Geology 115:1–19. https://doi.org/10.1086/509246
Syvitski JPM, Vörösmarty CJ, Kettner AJ, Green P (2005) Impact of humans on the flux of terrestrial sediment to the global coastal ocean. Science 308 (5720):376-380. https://doi.org/10.1126/science.1109454
Takata K, Emori S, Watanabe T (2003) Development of the minimal advanced treatments of surface interaction and runoff. Glob Planet Chang 38:209–222. https://doi.org/10.1016/S0921-8181(03)00030-4
Tan Z, Leung LR, Li H, Tesfa T (2018) Modeling sediment yield in land surface and Earth system models: Model comparison, development, and evaluation. Journal of Advances in Modeling Earth Systems 10:2192–2213. https://doi.org/10.1029/2017MS001270
United Nations Environment Programme (2018) GEMStat database of the Global Environment Monitoring System for freshwater (GEMS/Water) Programme. International Centre for Water Resources and Global Change, Koblenz. Accessed 10 Oct 2017. Available upon request from GEMS/Water Data Centre: gemstat.org
Walling DE (2006) Human impact on land–ocean sediment transfer by the world's rivers. Geomorphology 79:192–216. https://doi.org/10.1016/j.geomorph.2006.06.019
Walling DE, Fang D (2003) Recent trends in the suspended sediment loads of the world's rivers. Glob Planet Chang 39:111–126. https://doi.org/10.1016/S0921-8181(03)00020-1
Yamazaki D, De Almeida GAM, Bates PD (2013) Improving computational efficiency in global river models by implementing the local inertial flow equation and a vector-based river network map. Water Resour Res 49:7221–7235. https://doi.org/10.1002/wrcr.20552
Yamazaki D, Kanae S, Kim H, Oki T (2011) A physically based description of floodplain inundation dynamics in a global river routing model. Water Resour Res 47:1–21. https://doi.org/10.1029/2010WR009726
Yu Y, Shi X, Wang H, Yue C, Chen S, Liu Y, Hu L, Qiao S (2013) Effects of dams on water and sediment delivery to the sea by the Huanghe (Yellow River): The special role of water-sediment modulation. Anthropocene 3:72–82. https://doi.org/10.1016/j.ancene.2014.03.001
Zhang J, Huang WW, Liu MG, Cui JZ (1994) Eco-social impact and chemical regimes of large chinese rivers—a short discussion. Water Res 28:609–617. https://doi.org/10.1016/0043-1354(94)90011-6
Zhou Y, Jeppesen E, Li J, Zhang Y, Zhang X, Li X (2016) Impacts of Three Gorges Reservoir on the sedimentation regimes in the downstream-linked two largest Chinese freshwater lakes. Sci Rep 6:35396. https://doi.org/10.1038/srep35396

## Publisher's Note